Ultrastructural and hormonal changes related to harmaline-induced treatment in *Arabidopsis thaliana* (L.) Heynh. root meristem

Sara Álvarez-Rodríguez[a], David López-González[a], Manuel J. Reigosa[a], Fabrizio Araniti[b], Adela M. Sánchez-Moreiras[a*]

[a]*Departamento de Bioloxía Vexetal e Ciencias do Solo, Facultade de Bioloxía, Universidade de Vigo, Campus Lagoas-Marcosende s/n, 36310, Vigo, Spain*
[b]*Dipartimento di Scienze Agrarie e Ambientali - Produzione, Territorio, Agroenergia, Università Statale di Milano, Via Celoria nº2, 20133 Milano, Italy*

*Corresponding author: Adela M. Sánchez-Moreiras, Departamento de Bioloxía Vexetal e Ciencias do Solo, Facultade de Bioloxía, Universidade de Vigo, Campus Lagoas-Marcosende s/n, 36310, Vigo, Spain. *E-mail* address: adela@uvigo.es

Abstract

Harmaline is an indole alkaloid with demonstrated phytotoxicity and recognized pharmacological applications. However, no information is available concerning its mode of action on plant metabolism. Therefore, the present work evaluated bioherbicide mode of action of harmaline on plant metabolism of *Arabidopsis thaliana* (L.) Heynh. Harmaline induced a strong inhibitory activity on root growth of treated seedlings, reaching IC_{50} and IC_{80} values of 14 and 29 µM, respectively. Treated roots were shorter and thicker than control and were characterized by a shorter root meristem size and an increase of root hairs production. Harmaline induced ultrastructural changes such as increment of cell wall thickness, higher density and condensation of mitochondria and vacuolization, appearance of cell wall deposits, increment of Golgi secretory activity and higher percentage of aberrant nuclei. The ethylene inhibitor $AgNO_3$ reversed high root hair appearance and increment of root thickness, and *pTCSn::GFP* transgenic line showed fluorescence cytokinin signal in stele zone after harmaline treatment that was absent in control, whereas the auxin signal in the transgenic line DR5 was significantly reduced by the treatment. All these results suggest that the mode of action of harmaline could be involving auxin, ethylene and cytokinin synergic/antagonistic action.

Keywords: bioherbicide, hormones, indole alkaloid, mode of action, phytotoxicity.

Abbreviations

IC_0	Control
IC_{50}	Half maximal inhibitory concentration
IC_{80}	80% inhibitory concentration
PCIB	*p*-chlorophenoxyisobutyric acid
PCIB15	*p*-chlorophenoxyisobutyric acid 15 µM
PCIB30	*p*-chlorophenoxyisobutyric acid 30 µM
$AgNO_3$	Silver nitrate
GFP	Green fluorescent protein
DR5	Auxin responsive promoter DR5
TCSn	Two component signaling sensor new
TEM	Transmission electron microscopy
ACC	1-aminocyclopropane carboxylic acid
AVG	aminoethoxyvinyl glycine

1. Introduction

Weeds represent one of the most impacting constraints in agro-ecosystems, for being responsible of the reduction of crop productivity and quality (Oerke, 2006). Nowadays, synthetic herbicides, defined as chemical products that inhibit weed growth, play a leading role in crop protection in agricultural ecosystems. Their application is effective in short-term crop yields, but their massive use has induced pollution, causing contamination of freshwater ecosystems and increasing the incidence of herbicide-resistant weeds (Tranel and Wright, 2002; Villeneuve et al., 2011). Those conventional

herbicides are characterized by simple chemical structures, which facilitate their synthesis, lowering manufacturing and marketing costs. Moreover, it is known that most of the herbicides have a single molecular target, which means that they inhibit specific biochemical processes, severely altering plant metabolism (Duke, 2012). Further, this specificity represents the main factor of the rapid evolution of weed resistance. Therefore, environmentally friendly products with innovative modes of action or multitarget activity are needed to counteract the quick increase of herbicide resistance. As a source of new green herbicides or as a backbone for herbicide discovery programs, specialized plant metabolites are becoming an effective alternative to the classic synthetic herbicides (Duke et al., 2000; Araniti et al., 2015; Araniti et al., 2020).

Several researchers studied the effects of many natural compounds on plant growth and development, mainly focusing on the root system, where hormonal balance and crosstalk, especially auxin, cytokinins and ethylene, plays a pivotal role (Garay-Arroyo et al., 2012; Liu et al., 2017a).

Auxin and cytokinin, for example, are involved in lateral root development. Whereas auxin transport along the root is required for the formation of lateral root primordium (Reed et al., 1998), the exogenous cytokinin application represses lateral root initiation, demonstrating its antagonistic role with auxin in lateral root development (Wightman et al., 1980; Li et al., 2006). Moreover, it has been recently demonstrated that cytokinins receptors are pivotal for lateral root initiazion but they are not involved in adventitious root formation.

Ethylene is considered as a positive regulator of root hair growth. The loss of ethylene receptors ETR1 and EIN2 leads to inhibition of root hair formation (Vissenberg et al., 2020). Moreover, silver nitrate ($AgNO_3$) has proved to be a very potent inhibitor of ethylene action, and, as a consequence, an inhibitor in root hair development (Kumar et al., 2009). Several researches have suggested that both auxin and ethylene play important roles in root hair growth, acting synergistically and interconnected with complex signalling pathways (Lee and Cho, 2013; Qin and Huang, 2018; Vissenberg et al., 2020).

Several molecules have been characterized for their hormone similarity effects (i.e. stimulation of lateral root branching, increase in root hair density and length, etc.) and deeply investigated to understand their mode of action (Santos Wagner et al., 2021; Lupini et al., 2014).

Among these specialized metabolites, alkaloids and their derivatives (i.e. indole alkaloids, among others) have been widely studied for their role in plant-plant interaction and their strong phytotoxic potential, making them good candidates for the production of new natural and/or natural-like herbicides (Lei et al., 2021). For example, Na et al. (2011) demonstrated that the alkaloid narciclasine was a potent inhibitor of the auxin polar transport, altering PIN2 localization. The same authors reported that this alkaloid was altering the cytoskeleton dynamics affecting the subcellular auxin traffick (Hu et al., 2015).

Harmaline (1-methyl-7-methoxy-3,4-dihydro-beta-carboline) is an indole alkaloid belonging to natural β-carboline alkaloids, together with harmine, harmalol or harmol. Specifically, this compound is a specialized metabolite that can be found in *Peganum harmala* L. seeds (*Zygophyllaceae*) (Farouk et al., 2007), in *Banisteriopsis caapi*

(Callaway et al., 2011) and also in *Passiflora incarnata* L. (Hamid et al., 2017). Harmaline has been studied for its biological activity, including antidepressant and antiparasitic properties (Evans and Croft, 1987; Di Giorgio et al., 2004; Herraiz et al., 2010). However, only few information is available about its impact on plant metabolism (Shao et al., 2013).

Therefore, our study aimed to evaluate, using *Arabidopsis thaliana* as model species, the phytotoxic potential of harmaline, trying to elucidate its potential mode of action through a pharmacological and microscopic approach.

2. Materials and methods

2.1 Dose-response curves

Arabidopsis thaliana seeds were sterilized in 50% ethanol and 0.5% sodium hypochlorite, with 0.01% Triton X100, for 3 minutes. Then, seeds were washed three times with ultrapure water and finally kept in 0.1% agar solution at 4 ºC for 72 h to synchronize the germination. After this period, seeds were sown in square Petri dishes (100 x 100 x 15 mm) using plant agar (Duchefa, Holland) supplemented with 0.44% mix of macro and micronutrients (Murashige-Skoog, Sigma-Aldrich, Saint Louis, USA) and 1% sucrose.

Before being added to the enriched agar medium, harmaline (Sigma-Aldrich) was diluted in heated ultrapure water to get the following concentrations: *i*) for the first dose-response curve 0, 50, 100, 200, 400, 800, 1200 µM, *ii*) for the second dose-response curve 0, 2.5, 5, 10, 20, 40, 80 µM. Five replicates with 24 seeds per plate were sown for each treatment. Once sown, plates were vertically arranged in a growth chamber with the following conditions: 8 daylight hours (120 µmol m^{-2} s^{-1})/16 h of darkness, at a constant temperature of 22 ± 2 ºC and 55% relative humidity. After 14 days of treatment, root length and germination were measured for each seedling, and raw data were used to build a dose-response curve. Data obtained from dose-response curves were fitted through non-linear regression to calculate two key concentrations IC_{50} and IC_{80} (harmaline doses required for 50% and 80% inhibition of root length, respectively). For stereo-microscope image acquisition, at least 8 roots per treatment were randomly selected, to avoid a bias on the analyses, and photographed using a Nikon SMZ 1500 stereo-microscope. Number of lateral roots (NLR), number of adventitious roots (NAR), root thickness (RT), root hair density (RHD), root hair length (RHL) and the distance between root apex and the first root hair position (FRHD) were quantified in five replicates per root parameter using Image-Pro Plus 6.0 (Media Cybernetics).

2.2 Structural and ultra-structural Arabidopsis root analysis

A. thaliana seeds were sterilized as previously described and grown for 7 and 14 days in IC_0 (0 µM) and IC_{50} (14 µM) harmaline medium. After this time, the meristems of untreated (IC_0) and treated (IC_{50}) radicles were cut (1-2 mm) and immersed in a 0.1 M cacodylate buffer with 5% glutaraldehyde fixative (pH 7.2). Meristems were kept at 4 ºC for 4 h, and then washed three times (4 h each) with 0.1 M cacodylate buffer. Afterwards,

samples were immersed in cacodylate buffer with OsO_4 (2%) for 3 h and then in 10% acetone and 2% uranyl solution for 1 h.

Radicles dehydration was carried out by dipping the samples in increasing acetone concentrations from 50% to 100%. Finally, samples were embedded in Spurr resin (4 inclusions of 3 h each). After a 60 ºC polymerization, semi-thin cuts (0.7 µm) were stained with toluidine blue, and their structure was visualized using a Nikon Eclipse 800 optical microscope equipped with a Sight Nikon DS-U2 digital camera and NIS-Elements D 2.30 SP1 software.

For ultra-structural studies through electron microscopy, ultra-thin cuts (50-70 nm) were contrasted with uranyl acetate (2%) for 30 min and lead citrate for 12 min (Reynolds, 1963) to finally be washed with ultrapure water. Meristem root cuts were ultrastructurally analyzed using a JEOL JEM-1010 (80kv) transmission electron microscope, equipped with a CCD Orius and Digital Montage Plug-in (Gatan Inc., Gatan, CA, USA) camera, as well as with "Gatan Digital Micrograph" (Gatan Inc.).

Meristem width (µm), cell wall thickness (µm), Golgi apparatus secretory activity (nº of vesicles per Golgi), percentage of aberrant nuclei (number of aberrant nuclei / 10 cells x 100), the density of mitochondria (number of mitochondria per cell), density of altered mitochondria (nº altered mitochondria per cell), density of vacuoles (nº vacuoles per cell) and percentage of cells with wall deposits (nº of cells with wall deposits / 10 cells x 100) were quantified in 10 images randomly chosen for the ultra-thin cuts.

2.3 Reversion bioassay with the anti-auxin p-chlorophenoxyisobutyric acid (PCIB)

The *p*-chlorophenoxyisobutyric acid (PCIB) (Sigma-Aldrich) is known as a synthetic anti-auxin widely used to inhibit auxin response (Oono et al., 2003). *Arabidopsis* seedlings were exposed to IC_{50} harmaline, to two different concentrations of PCIB (15 and 30 µM), and to a mixture of PCIB15 + IC_{50} harmaline and PCIB30 + IC_{50} harmaline. Harmaline was diluted into the liquid agar by heat dilution with ultrapure water, and PCIB was directly added to the corresponding plates. Seedlings were visualized under a Nikon SMZ 1500 stereo-microscope after 7 and 14 days of growth. The number of lateral roots (NLR), the number of adventitious roots (NAR), root thickness (RT), root hair density (RHD), root hair length (RHL) and the distance between root apex and the first root hair position (FRHD) were quantified in five replications per treatment. Root parameters were quantified using Image-Pro Plus 6.0 (Media Cybernetics).

2.4 Reversion bioassay with the ethylene inhibitor $AgNO_3$

Silver nitrate ($AgNO_3$) is known to be a very potent inhibitor of ethylene action, and it is widely used for plant growth regulation, plant tissue culture, and *in vivo* and *in vitro* morphogenesis (Kumar et al., 2009). Two bioassays were done using different harmaline concentrations. A first bioassay was done using IC_{50} harmaline and 10 µM $AgNO_3$, whereas in the second bioassay, *Arabidopsis* seedlings were grown in agar plates with 0, 2.5, 5, 10 and 20 µM harmaline concentrations, 10 µM $AgNO_3$, and a mixture of both $AgNO_3$ and each harmaline concentration (0, 2.5, 5, 10 and 20 µM). After 7 and 14 days of treatment, seedlings were morphologically analyzed under a Nikon SMZ 1500 stereo-microscope and five replications per treatment were used to quantify the number of lateral

roots (NLR), number of adventitious roots (NAR), root thickness (RT), root hair density (RHD), root hair length (RHL) and the distance between root apex and the first root hair position (FRHD). Root parameters were quantified using Image-Pro Plus 6.0 (Media Cybernetics).

2.5 Bioassays with GFP transgenic lines

Arabidopsis GFP transgenic lines were used in this study. In particular, the synthetic auxin response promoter (*pDR5::GFP*) (Ottenschläger et al., 2003) and the cytokinin sensor mutant (*pTCSn::GFP*) (Liu and Müller, 2017b) were used. *pTCSn::GFP* seedlings were exposed to 0 μM and IC_{50} concentration, whereas *pDR5::GFP* was exposed to different concentrations of harmaline (0, 2.5, 5, 10, 13, 16, 19, and 20 μM).

After 14 days of growth, root caps of *pDR5::GFP* were observed and photographed using a Leica TCS SP5 microscope (Wetzlar, Germany). The GFP signal was measured using an excitation wavelength settled at 488 nm and an emission wavelength of 509 nm. Images were recorded with 63X oil immersion lenses. *pTCSn::GFP* transgenic line images were taken using a 20X lens in an epifluorescence microscope (Olympus BX53).

2.6 Statistical analysis

The dose-response curve experiments were carried out using a completely randomized design with five replications (each replicate was a bulk of 24 plants). IC_{50} and IC_{80} values were calculated through non-linear regression, selecting for curve fitting the equation with the higher R^2 (>0.9). For ethylene inhibitor ($AgNO_3$) and anti-auxinic (PCIB) assays, five replications per treatment were used in order to quantify each root parameter. An exploratory data analysis was carried out in order to detect *outliers*. Data were first checked for deviation from normality, using the Kolmogorov-Smirnov test, and then tested for homogeneity using the Levene test. Data were then analyzed through one way-ANOVA using the Least Significant Differences (LSD, $p \leq 0.05$) test as post-hoc. Different letters indicate significant differences between treatments.

The comparison between treatments for ultra-structural changes quantification (meristem zone width, cell wall thickness, Golgi apparatus secretory activity, percentage of aberrant nuclei, density of mitochondria, density of vacuoles and percentage of cell with wall deposits) was done with *t*-test ($P \leq 0.05$). Asterisks indicate significant differences compared to the control: * ($P \leq 0.05$), ** ($P \leq 0.01$), *** ($P \leq 0.001$).

Data were analyzed using IBM SPSS Statistics v. 25.0 software (SPSS, Chicago)

3. Results

3.1 Dose-response curves and root morphology

The experiment carried out using a dose-response curve, built on harmaline ranging from 0 to 1200 μM, pointed out that concentrations higher than 50 μM significantly stunted root growth (Fig. 1C, D). Moreover, doses higher than 800 μM completely inhibited the germination process (Fig. S1). Therefore, to better identify the IC_{50} and IC_{80} values, a new dose-response curve was done using seven concentrations ranging from 0

μM to 80 μM. The results highlighted that phytotoxic activity was so effective that IC_{50} and IC_{80} values were reached at concentrations as low as 14 and 29 μM, respectively.

Harmaline-treated seedlings were visualized under a stereo-microscope in order to study morphological effects caused by the compound. After 14 days of growth, the control seedlings showed uniform morphology and thickness of roots with a homogeneous arrangement of their cells in symmetrical rows, as shown by the light microscopic images (Fig. 2).

In contrast, harmaline induced a dose-dependent phytotoxic effect significantly altering *Arabidopsis* root morphology. In particular, treated plants were characterized by a significant increment of root hair density (RHD) when comparing with untreated seedlings (0.016) already at concentrations lower than 5 μM (0.027). This increment became higher for increasing concentrations (Fig. 2D). A significant reduction in the number of lateral roots (NLR) at concentrations ≥ 5 μM (3.13 folds lower than control) was also observed (Fig. 2B). Harmaline also induced a significant increment (3 folds higher than control) in root thickness (RT) at concentrations ≥ 10 μM (Fig. 2F). In addition, root hairs length (RHL) was significantly inhibited by the treatment (1.3 folds lower than control) at the highest concentrations assayed (40, 80 μM) (Fig. 2C). The distance from the apex to the appearance of the first root hair (FRHD) decreased with increasing concentrations, showing that the distance was 2 folds lower than control roots already at 10 μM and up to 9 folds lower at the highest concentrations (40 and 80 μM) (Fig. 2A).

3.2 Harmaline effects on root cells anatomy and ultra-structure

Compared to 7 days (Fig. 3A) and 14 days control roots (Fig. 3C), light microscopic images showed that seedlings exposed to IC_{50} harmaline were characterized by a reduction in root meristem size and a significant increment of its width (3.1 and 3.9 folds higher than the control, after 7 and 14 days, respectively) (Fig. S2). Moreover, the meristematic and maturation zones were characterized by hyper-elongated and abnormal epidermal, cortex and endodermal cells, and an increase in the size of the procambium and stele cells (Fig. 3B; Fig. 3D).

The effects observed under stereo and light microscopy were further confirmed by TEM. The meristematic cells of control roots showed a uniform morphology characteristic of healthy cells: large nuclei with lax chromatin (Fig. 4C; Fig. 4G), cell wall with homogeneous thickness, and cellular organelles (mitochondria, Golgi apparatus, among others) with the typical morphology, size, shape, and location (Fig. 4D; Fig. 4E; Fig. 4H; Fig. 4I). By contrast, seedlings treated with IC_{50} harmaline experienced characteristic ultrastructural changes after both 7 and 14 days of treatment. The strong thickening observed under stereo- and optical-microscopy was also observed under electron microscopy (Fig. 5 and Fig. 6).

The ultrastructural analysis carried on untreated and harmaline-treated roots pointed out a significant alteration of the root cell structure and organization, revealing many ultrastructural changes. Cell shapes, cell walls and several organelles, such as nuclei, vacuoles, mitochondria, were affected by harmaline treatment (Table 1, Fig. 5B-F and Fig. 6D-G).

Compared to control cells, the density of vacuoles was around 14 folds higher after 7 and 14 days of IC_{50} harmaline exposure. In addition, vacuoles of untreated seedlings were characterized by a small defined dimension surrounded by a highly recognizable tonoplast (Fig. 4H), and the tonoplast of several vacuoles in the harmaline-treated root meristems was blurry and not easily distinguishable (Fig. 5C, Fig. 5D, Fig. 5F, and Fig. 6F). In harmaline-treated root cells, a high number of vacuoles presented aggregations of granular precipitates located peripherally or throughout the organelle (Fig 5F). In addition, vacuoles with irregular membrane-bound structures with dense granulose material and a high number of vacuoles in autolytic activity were commonly found (Fig 5A, Fig. 5F, Fig. 6A-B, and Fig. 6G).

Concerning the nuclei, significant differences between the percentage of aberrant nuclei were observed for untreated (21.89%) and harmaline treated cells after 7 days (56.62%) and 14 days of growth (60%) (Table 1; Fig 5B). No differences between control and treated cells were observed in the Golgi apparatus morphology. However, after 14 days of treatment, harmaline-treated cells showed significant differences in the number of vesicles in the surrounding of the Golgi apparatus, suggesting an increase of its secretory activity (13.1 folds higher than the control) (Table 1; Fig S3).

Furthermore, harmaline-treatment induced an alteration of cell shape, probably due to the significant increase of cell wall thickness, which was 2.4 folds higher than control after 7 days of treatment, and 6 folds higher after 14 days of IC_{50} treatment (Table 1). Moreover, cell corners appeared swollen, with an abnormal shape and electrodense deposits (Fig. 6G). In particular, the number of cell wall deposits after 7 days of treatment was 3.2 folds higher than the control after 7 days and 3.6 folds higher after 14 days of treatment.

Alterations in mitochondria morphology and density were also commonly observed in harmaline-treated cells. While control cells were characterized by pleomorphic mitochondria, delimited by a discernible double membrane containing numerous cristae in a dense stroma (Fig 4D-E and Fig. 4H-I), harmaline-treated mitochondria were characterized by significant shape alterations (from oval to spherical) with translucent stroma and/or without cristae. In particular, the condensation of altered mitochondria was 4.3 and 6.6 folds higher than control after 7 and 14 days of harmaline treatment, respectively (Fig. 5D-F; Table 1). Regarding mitochondrial density (number of mitochondria per cell), a higher number was found in harmaline-treated cells (21) than in control cells (15.2) after 7 days of treatment. This difference was also found between control (12.5) and treated cells (17.6) in 14 days treated seedlings (Table 1).

3.3 Pharmacological approach: auxin (PCIB) and ethylene ($AgNO_3$) inhibitors

Based on the previously observed effects (especially the increase of root hair density, length and the shortening of root meristem), reversion bioassays with hormonal inhibitors were done in 14 days treated roots to observe both auxin and ethylene roles in harmaline mode of action.

Regarding the anti-auxinic bioassay, as shown in Fig. 7A, control seedlings experienced uniform growth with no apparent abnormalities and a normal number and arrangement of root hairs for 14 days. Similar shape and appearance were obtained for seedlings treated

only with PCIB (Fig. 7B; Fig. 7C). As expected, plants treated with IC_{50} harmaline showed a massive appearance of root hairs in the whole root (the root hair density of treated roots was 2.7 folds higher than the control). After anti-auxinic addition, root hair density was reduced 1.3 fold compared to harmaline treatment (Fig. 7E; Fig. 7F; Table S1). Regarding to meristematic zone width, there was also a 3.2-folds increment for harmaline-treated roots, as was already observed in previous bioassays (Fig. 7D). On the contrary, in seedlings grown with the combined IC_{50} harmaline + PCIB (15 and 30 μM), PCIB addition was able to reverse the appearance of lateral roots (2.8 folds lower after anti-auxinic addition), and root thickening in all cases, with reductions of 3.7 and 3.1 folds after addition of 15 and 30 μM PCIB, respectively, when compared to harmaline treatment; Table S1). Regarding root hair length, no significant differences were found among treatments.

Given the emergence of root hairs despite the anti-auxinic treatment (the root hair density was 2.1 folds higher in seedlings grown with IC_{50} harmaline + PCIB than control seedlings; Table S1), an ethylene inhibitor bioassay was carried out to check the possible implication of ethylene on the mode of action of harmaline. Control seedlings displayed a well-organized main root with root hairs next to the hypocotyl and an apex with normal thickness and appearance after 14 days (Fig. 7G). In contrast, as already observed in PCIB assay, seedlings treated with the IC_{50} harmaline showed an increased number and length of root hairs, which appeared over the whole root, from the beginning of the hypocotyl to the end of the apex (Fig. 7H). Moreover, the shortening and thickening of roots affected all treated seedlings, and there was also a reduction in the number of lateral roots (2 folds lower compared to control).

However, combined harmaline plus ethylene inhibitor treatment (IC_{50} + $AgNO_3$) reversed the massive appearance of root hairs already at 7 days of growth. After 14 days of treatment, silver nitrate completely reversed the massive growth of root hairs, with 3.3 folds lower RHD after ethylene inhibitor addition, and root thickening (2.9 folds lower in the presence of silver nitrate) (Fig. 7I; Table S1). Seedlings exposed to IC_{50} + $AgNO_3$ also displayed a noticeable proliferation of lateral roots characterized by a typical morphology (no harmaline-induced alterations were observed). In addition, significant differences between radicle lengths of IC_{50} harmaline and IC_{50} + $AgNO_3$ treated seedlings were found after 14 days of growth. Plants treated with harmaline in combination with silver nitrate showed a significantly higher growth compared to roots grown only with harmaline (21.7 mm *vs* 7.85 mm, respectively; Table S1).

Significant differences were also found on root thickness between seedlings grown with IC_{50} harmaline and those grown with IC_{50} + $AgNO_3$ (411 mm *vs* 139 mm, respectively). In fact, no differences were found between the root thickness of control and harmaline-treated roots when silver nitrate was also present. In summary, ethylene inhibitor successfully reversed harmaline effects in treated roots.

A new $AgNO_3$ reversion bioassay was conducted with increasing harmaline concentrations, given the results obtained in the previous bioassay. At the lower concentrations (2.5, 5 and 10 μM), $AgNO_3$ reversed the massive root hairs appearance all over the root (no significant differences were found in RHD after $AgNO_3$ addition between untreated roots and those treated with 2.5, 5 and 10 μM harmaline) (Fig. 8D; Fig.

8F; Fig. 8H). The higher concentration assayed (20 μM) showed a 2.8 folds-higher root hair density than control roots, but after ethylene inhibitor addition, the RHD was 2.3 folds lower than untreated roots (Table S2). Moreover, concerning root thickness, $AgNO_3$ was able to revert this parameter only for harmaline concentrations lower than 10 μM (Fig. 8H; Table S2). However, these effects became increasingly noticeable with the higher concentration tested (20 μM). While 20 μM harmaline seedlings displayed a massive appearance of root hairs and shortened and thicker roots, those grown together with $AgNO_3$ did not develop root hairs, although root thickening was still present, being 3 folds higher than control roots after the addition of the ethylene inhibitor (Fig. 8J; Table S2).

In summary, after 14 days of growth, most of the characteristic harmaline effects completely disappeared in the presence of the ethylene inhibitor; i.e. root thickening faded out, root hairs only grew close to the hypocotyl, and root apex was equal to control seedlings. $AgNO_3$ did not reverse root thickening at the highest concentration tested (20 μM) but significantly reduced root hairs proliferation (2.3 folds lower than control) (Table S2).

3.4 Bioassays with GFP transgenic lines

To get a closer view of the structure of harmaline-treated roots and the role of other hormones on harmaline mechanisms, *pTCSn::GFP* and *pDR5::GFP* transgenic lines were visualized under confocal microscopy after 14 days of treatment. Cytokinin distribution was observed all over the meristematic zone (Fig. 9). Control seedlings showed homogeneous fluorescence signal in apical meristem after 14 days growth (Fig. 9A), whereas samples treated with IC_{50} harmaline showed an expanded fluorescence signal in the stele (Fig. 9B).

Concerning the *pDR5::GFP* transgenic line, two different bioassays were carried out. The first bioassay, settled using five different harmaline concentrations (0, 2.5, 5, 10 and 20 μM) (Fig. 10A-E, respectively), showed almost complete disappearance of the fluorescence between 10 μM (where auxin presence could be appreciated; Fig. 10D) and 20 μM (where fluoresce signal became insignificant; Fig. 10E). For this reason, new concentrations were tested (0, 10, 13, 16 and 19 μM; Fig. 10F-J, respectively) to deepen the effects of harmaline on DR5 signal in the range between 10 and 19 μM.

In contrast to control roots, which showed a homogeneous signal without abnormalities, harmaline-treated seedlings displayed an increment in fluorescence signal as harmaline concentration increased. However, the auxin signal disappeared between 16 μM and 19 μM, at a concentration already higher than the IC_{50} value for harmaline (Fig. 10I; Fig. 10J; Fig. S5).

4. Discussion

Harmaline significantly altered root morphology of *Arabidopsis* seedlings, affecting root cell anatomy and ultra-structure at low concentrations. In fact, IC_{50} and IC_{80} values (14 and 29 μM, respectively) were lower than several phytotoxic specialized metabolites

reported in the literature (Díaz-Tielas et al., 2012; Graña et al., 2017; López-González et al., 2020; Landi et al., 2020).

In plants treated with harmaline, the root meristem was characterized by decreased length and strongly increased width, suggesting an early differentiation of meristematic cells. Similar effects were observed in Arabidopsis seedlings treated with the hormone-like compound brassinolide and with cadmium, in which a premature cell cycle exit determined an early differentiation of meristematic cells (Bruno et al., 2017; González-García et al., 2011). Similarly to these two compounds, harmaline treatment reduced the apical root meristem size and overall root growth.

In fact, the root morphology of plants treated with harmaline was characterized by a decrese of primary root length and lateral root number. In contrast, the number of adventitious roots was significantly increased in harmaline treated roots at concentrations higher than 20 µM, which strongly damaged the root meristem.

The reduction of root meristem and lateral root production was previously observed by Dello Ioio et al. (2007) in Arabidopsis seedlings treated with increasing doses of exogenous cytokinins. In fact, it is largely known that exogenous cytokinin application is negatively correlated with lateral and adventitious root production and that this phenomenon is driven by an alteration of auxin/cytokinin balance (Jing and Strader, 2019). However, the number of adventitious roots was significantly increased at harmaline concentrations higher than 20 µM, which strongly damaged the root meristem blocking its growth and altering its anatomy. This increase in adventitious roots could probably be due to significant damages to the root meristem accompanied by the loss of functionality of the primary root, which is known to stimulate adventitious root production (Gonin et al., 2019).

The increase in root meristem thickness, observed in harmaline-treated roots, was accompanied by an increment of root hair density, which, as described by the FRHD parameter, was found extremely close to the meristematic zone, suggesting that the primary meristem was defective and consumed (Zhang et al., 2015).

Similar effects on root morphology were observed with other natural compounds, such as coumarin, norharmane, scopoletin and protodioscin (López-González et al., 2020; Bruno et al., 2021; Santos Wagner et al., 2021). For example, norharmane induced the formation of ectopic root hairs and adventitious roots compared to untreated roots after 14 days of exposure. Similarly, scopoletin treated plants were characterized by the proliferation of root hairs close to the root tip, and protodioscin caused a thickening of the meristematic root area and an increase in root hair density. All these compounds were suggested to interact with plant hormones biasing their biosynthesis and distribution (Bruno et al., 2021; López-González et al., 2020; Santos Wagner et al., 2021).

In addition, root swelling and root hair over-production are typical symptoms observed on plants treated with commercial auxinic herbicides, which are known to induce, as primary symptoms, an increase of ethylene and a reduction of auxin transport (Grossmann, 2010), further supporting the hypothesis that harmaline could interfere with the seedlings' hormonal balance.

Since anatomical macro alterations are generally correlated with cell ultrastructure, we decided to investigate the effects of this natural molecule on Arabidopsis root tips, which was an organ severely affected and pivotal for root development.

The ultrastructural alterations observed in harmaline-treated plants were similar to those observed with other phytotoxic natural compounds and synthetic herbicides. In particular, the sesquiterpene farnesene and the indole-alkaloid norharmane affected primary root cells ultra-structure, causing similar effects to those observed with harmaline (i.e. abnormal cell shape, altered mitochondria, autolytic activity, high amount of cell corner deposit, among others) (Araniti et al., 2016; López-González et al., 2020). Concerning farnesene, the authors suggested that those effects were induced by a biased production of auxin and ethylene (Araniti et al., 2016). Successively they demonstrated that the peculiar phenotype of farnesene treated roots was mainly due to a biased distribution of auxin due to an alteration of efflux transporters (Araniti et al., 2017). Ultrastructural effects induced by scopoletin also coincided with those showed after harmaline exposure (increment of cytoplasm vacuolization and secretory Golgi activity and accumulation of deposits at cell walls). The authors suggested that these effects could be related to detoxification processes due to the impact of toxic compounds and that scopoletin could behave as an auxin herbicide because of its similarities with other auxin analogues such as 2,4-D (Graña et al., 2017).

Moreover, similar ultrastructure alterations were also observed in plants treated with synthetic herbicides such as amiprophos-methyl, metsulfuron-methyl and chlorsulfuron (Fayez et al., 1994; Fayez and Kristen, 1996; Kundelchuk et al., 2002). As also observed in harmaline treated cells, these two herbicidal molecules increased the number and size of vacuoles, characterized by a high accumulation of electrodense deposits.

As previously reported, TEM and light microscopy pointed out that harmaline-treated seedlings experienced shortening of the meristematic zone and strong cell differentiation after 7 and 14 days of exposure.

Because of the similarity of harmaline effects with those observed with several natural compounds interfering with the hormonal balance, the effects of this indole alkaloid were analysed using transgenic GFP lines and a pharmacological approach.

After 14 days of harmaline exposure (14 μM) the cytokinin sensor *pTCSn::GFP* showed an expanded fluorescence signal in both root cap and stele. On the contrary, the signal was only observable in the root tip at the quiescent center and columella level in control seedlings. Bishopp et al. (2011) demonstrated that cytokinin is transported through the xylem and phloem. Together with the ability of harmaline to be assimilated, transported and accumulated in roots and shoots (Fig. S4), these results are consistent with the hypothesis that cytokinins could also be involved in the harmaline mode of action. In the last few years, cytokinin and auxin have been related to their interaction in plant development (Moubayidin et al., 2009; Su et al., 2011). Both are known to be involved synergistically or antagonistically in many plant growth processes such as meristem formation, signaling, or gene expression (El-Showk et al., 2013; Schaller et al., 2015). The pioneering study of Skoog and Miller (1957) in *in-vitro* plant tissues indicated that root and shoot development depended on the auxin/cytokinin ratio; i.e. high levels of cytokinin supported shoot formation, whereas high concentrations of auxin promoted

rooting. Auxin and cytokinin act antagonistically in root development by regulating their synthesis, transport, and response. While auxin promotes cell division, cytokinin promotes meristematic cell differentiation in vascular tissue, reducing root meristem size and accelerating shoot growth (Dello Ioio et al., 2008).

However, cytokinin also represses auxin transport and responses in the differentiation-elongation limit of the meristem (Chapman and Estelle, 2009). Dello Ioio et al. (2008) found that cytokinin and auxin antagonistically interact by controlling in opposite ways *SHY2* protein abundance; cytokinin inhibited auxin transport through activating transcription of *SHY2* gene, which reduced PIN expression in the vascular transition zone, while exogenous auxin (3-indoleacetic acid) application to *Arabidopsis* roots caused an increment of meristem size. In summary, auxin-cytokinin antagonistic effects are necessary to balance cell differentiation in the transition zone, caused by cytokinin (Dello Ioio et al., 2007) and cell division, mediated by auxin (Blilou et al., 2005).

Therefore, auxin-cytokinin crosstalk could explain some of the effects observed after harmaline treatment. Regarding the results obtained with the transgenic line *pDR5::GFP*, which marks an auxin-responsive promoter with fluorescence, harmaline-treated seedlings showed complete disappearance of auxin fluorescence signal between 16 and 19 μM (Fig. S5). These results suggest a relationship between harmaline treatment and auxin disappearance in treated seedlings. Auxin disappearance occurs when seedlings are treated with higher concentrations than IC_{50} harmaline (14 μM), after phenotypical effects of harmaline can be detected, like shortening of meristematic size and root thickening due to the highly differentiated cells number, and after cytokinin is accumulated in the transition zone. This could confirm that auxin disappearance would not be the cause but the consequence of the mode of action of harmaline. It could not be the primary mechanism of action but a secondary effect. Auxin-cytokinin crosstalk could be responsible for the mode of action of harmaline, which would increase endogenous cytokinin signal resulting in auxin signaling disappearance in the root tip at higher concentrations than 20 μM.

Another effect induced by harmaline is the massive appearance of root hairs. It was demonstrated that seedlings treated with increased concentrations of 1-aminocyclopropane carboxylic acid (ACC), the ethylene precursor, have developed a high number of root hairs in ectopic positions (Tanimoto et al., 1995), while *Arabidopsis* seedlings grown with high concentrations of aminoethoxyvinyl glycine (AVG), an ethylene biosynthesis inhibitor, did not develop any root hairs. Dolan et al. (2001) also suggested that ethylene is associated with the positioning of the site root hair initiation.

Given the high presence of root hairs in harmaline-treated roots, $AgNO_3$, a potent inhibitor of ethylene action (Beyer, 1976; Kumar et al., 2009), was used to demonstrate if ethylene was implicated in its mode of action. Silver nitrate reversed massive root hairs appearance when applied in combination with IC_{50} harmaline. In addition, harmaline+$AgNO_3$ treated seedlings displayed lateral root proliferation. Previous studies with *Arabidopsis* and tomato showed that ethylene inhibited lateral root formation (Negi et al., 2008; Negi et al., 2010). In this way, an absence of ethylene would enhance lateral root proliferation, as obtained for harmaline+$AgNO_3$ treated seedlings.

Cytokinin plays an important role in ethylene biosynthesis regulation. Previous studies suggested that cytokinin treatment increased ethylene biosynthesis in *Arabidopsis* seedlings by post-transcriptional mechanisms (Vogel et al., 1998; Woeste et al., 1999). Auxin, cytokinin and ethylene are connected with an expanded network and concentrations of all three hormones are regulated by a hormonal crosstalk. If a given hormone suffers any change in concentration/response, the other two hormones may also change their concentrations/responses (Liu et al., 2013). Any perturbation in the network induced by harmaline exposure, could cause changes in other components. In this way, this study suggests that root hair massive proliferation could be related to ethylene action, that could be involved in the mode of action of harmaline with auxin and cytokinin.

5. Conclusions

The natural compound harmaline caused morphological and ultrastructural changes in *Arabidopsis thaliana* roots, such as increment of root hair production and root thickness, or increment of cell wall thickness, Golgi secretory activity, mitochondria density and vacuolization. The results of this study suggest that the hormones cytokinin, auxin and ethylene could be involved in the mode of action of the natural compound harmaline. Harmaline may be acting by inducing cytokinin/auxin unbalance in the root meristem, affecting the processes involved in root meristem and causing ethylene alteration, responsible of massive root hair proliferation. Further analyses on the biosynthesis of cytokinin and auxin would help to understand the role of these hormones on the mode of action of harmaline.

Authors contribution

SAR, MJR and ASM planned the experiments. SAR, DLG and FA performed the experiments. SAR, FA and ASM analyzed the data and wrote the manuscript.

Acknowledgements

The authors would like to thank Inés Pazos at the Scientific and Technological Research Support Centre (CACTI) of the Universidade de Vigo for assisting in electron and confocal microscopy services. Moreover, we would like to thank Prof. Ikram Blilou and Prof. Bruno Müller which gently provided the mutated lines used in the experiments.

Funding

These results are part of the I+D+i project RTI2018-094716-B-100 funded by MCIN/AEI/10.13039/501100011033.

Declaration of competing interest

The authors declare no known competing financial interests or personal relationships that could have influenced the scientific work reported.

References

Araniti, F., Mancuso, R., Lupini, A., Giofrè, SV., Sunseri, F., Gabriele, B., Abenavoli, MR., 2015. Phytotoxic potential and biological activity of three synthetic coumarin derivatives as new natural-like herbicides. Molecules 20 (10), 17883-17902.

Araniti, F., Graña, E., Krasuska, U., Bogatek, R., Reigosa, MJ., Abenavoli, MR., Sánchez-Moreiras, AM., 2016. Loss of gravitropism in farnesene-treated *Arabidopsis* is due to microtubule malformations related to hormonal and ROS unbalance. PloS one. 11(8), e0160202.

Araniti, F., Bruno, L., Sunseri, F., Pacenza, M., Forgione, I., Bitonti, MB., Abenavoli, MR., 2017. The allelochemical farnesene affects *Arabidopsis thaliana* root meristem altering auxin distribution. Plant Physiol. Biochem. 121, 14-20.

Araniti, F., Mancuso, R., Lupini, A., Sunseri, F., Abenavoli, MR., Gabriele, B., 2020. Benzofuran-2-acetic esters as a new class of natural-like herbicides. Pest Manag. Sci. 76 (1), 395-404.

Beyer, EM., 1976. A potent inhibitor of ethylene action in plants. Plant Physiol. 58, 268–271.

Bishopp, A., Lehesranta, S., Vatén, A., Help, H., El-Showk, S., Scheres, B., Helariutta, K., Mähönen, AP., Sakakibara, H., Helariutta, Y., 2011. Phloem-transported cytokinin regulates polar auxin transport and maintains vascular pattern in the root meristem. Curr. Biol. 11, 927-932.

Blilou, I., Xu, J., Wildwater, M., Willemsen, V., Paponov, I., Friml, J., Heidstra, R., Aida, M., Palme, K., Scheres, B., 2005. The PIN auxin efflux facilitator network controls growth and patterning in *Arabidopsis* roots. Nature 433, 39-44.

Bruno, L., Pacenza, M., Forgione, I., Lamerton, LR., Greco, M., Chiappetta, A., Bitonti, MB., 2017. In Arabidopsis thaliana cadmium impact on the growth of primary root by altering SCR expression and auxin-cytokinin cross-talk. Front. Plant Sci. 8, 1323.

Bruno, L., Talarico, E., Cabeiras-Freijanes, L., Madeo, ML., Muto, A., Minervino, M., Lucini, L., Miras-Moreno, B., Sofo, A., Araniti, F, 2021. Coumarin interferes with polar auxin transport altering microtubule cortical array organization in *Arabidopsis thaliana* (L.) Heynh. Root apical meristem. Int. J. Mol. Sci. 22, 7305.

Callaway, JC., Brito, GS., Neves, ES., 2011. Phytochemical analyses of *Banisteriopsis caapi* and *Psychotria viridis*. J. Psychoact. Drugs 37 (2), 145-150.

Chapman, EJ., Estelle, M., 2009. Cytokinin and auxin intersection in root meristems. Genome Biol. 10, 210.

Dello Ioio, R., Linhares, FS., Scacchi, E., Casamitjana-Martinez, E., Heidstra, R., Costantino, P., Sabatini, S., 2007. Cytokinins determine *Arabidopsis* root-meristem size by controlling cell differentiation. Curr. Biol. 17, 678-682.

Dello Ioio, R., Nakamura, K., Moubayidin, L., Perilli, S., Taniguchi, M., Morita, MT., Aoyama, T., Costantino, P., Sabatini, S., 2008. A genetic framework for the control of cell division and differentiation in the root meristem. Science 322, 1380-1384.

Di Giorgio, C., Delmas, F., Ollivier, E., Elias, R., Balansard, G., Timon-David, P., 2004. In vitro activity of the β-carboline alkaloids harmane, harmine, and harmaline toward parasites of the species *Leishmania infantum*. Exp. Parasitol. 106, 67–74.

Díaz-Tielas, C., Graña, E., Sotelo, T., Reigosa, MJ., Sánchez-Moreiras, AM., 2012. The natural compound trans-chalcone induces programmed cell death in *Arabidopsis thaliana* roots. Plant Cell Environ. 35, 1500-1517.

Dolan, L., 2001. The role of ethylene in root hair growth in *Arabidopsis*. J. Plant Nutr. Soil Sci. 164 (2), 141–145.

Duke SO., Romagni, J., Daya, F., 2000. Natural products as sources for new mechanisms of herbicidal action. Crop Prot. 19, 583-589.

Duke, SO., 2012. Why have no new herbicides modes of action appeared in recent years? Pest Manag. Sci. 68, 505-512.

El-Showk, S., Ruonala, R., Helariutta, Y., 2013. Crossing paths: cytokinin signaling and crosstalk. Development 140, 1373-1383.

Evans, AT., Croft, SL., 1987. Antileishmanial activity of harmaline and other tryptamine derivatives. Phytother. Res. 1 (1), 25–27.

Farouk, L., Laroubi, A., Aboufatima, R., Benharref, A., Chait, A., 2007. Evaluation of the analgesic effect of alkaloid extract of *Peganum harmala* L.: possible mechanisms involved. J. Ethnopharmacol. 115 (3), 449–454.

Fayez, KA., Gerken, I., Kristen, U., 1994. Ultrastructural responses of root caps to the herbicides chlorsulfuron and metsulfuron methyl. Plant Soil, 167 (1), 127-134.

Fayez, KA., Kristen, U., 1996. The influence of herbicides on the growth and proline content of primary roots and on the ultrastructure of root caps. Environ. Exp. Bot. 36 (1), 71-81.

Garay-Arroyo, A., De La Paz Sánchez, M., García-Ponce, B., Azpeitia, E., Álvarez-Buylla, ER., 2012. Hormone symphony during root growth and development. Dev. Dyn. 241 (12), 1867-1885.

Gonin, M., Bergougnoux, V., Nguyen, TD., Gantet, P., Champion, A., 2019. What Makes Adventitious Roots? Plants, 8, 240.

González-García, MP., Vilarrasa-Blasi, J., Zhiponova, M., Divol, F., Mora-García, S., Russinova, E., Caño-Delgado, AI., 2011. Brassinosteroids control meristem size by promoting cell cycle progression in Arabidopsis roots. Development 138 (5), 849-859.

Graña, E., Sotelo, T., Díaz-Tielas, C., Araniti, F., Krasuska, U., Bogatek, R., Reigosa, MJ., Sánchez-Moreiras, AM., 2013. Citral induces auxin and ethylene-mediated malformations and arrests cell division in *Arabidopsis thaliana* roots. J. Chem. Ecol. 39, 271-282.

Graña, E., Costas-Gil, A., Longueira, S., Celeiro, M., Teijeira, M., Reigosa, MJ., Sánchez-Moreiras, AM., 2017. Auxin-like effects of the natural coumarin scopoletin on *Arabidopsis* cell structure and morphology. J. Plant Physiol. 218, 45-55.

Grossmann, K., 2010. Auxin herbicides: current status of mechanism and mode of action. Pest Manag. Sci. 66 (2), 113-120.

Hamid, HA., Ramli, ANM., Yusoff, MM., 2017. Indole alkaloids from plants as potential leads for antidepressant drugs: a mini review. Front. Pharmacol. 8 (96).

Herraiz, T., González, D., Ancín-Azpilicueta, C., Arán, VJ., Guillén, H., 2010. β-Carboline alkaloids in *Peganum harmala* and inhibition of human monoamine oxidase (MAO). Food Chem. Toxicol. 48 (3), 839–845.

Hu, Y., Na, X., Li, J., Yang, L., You, J., Liang, X., Wang, J., Peng, L., Bi, Y., 2015. Narciclasine, a potential allelochemical, affects subcellular trafficking of auxin transporter proteins and actin cytoskeleton dynamics in Arabidopsis roots. Planta, 242 (6), 1349-1360.

Jing, H., Strader, LC., 2019. Interplay of Auxin and Cytokinin in Lateral Root Development. Int. J. Mol. Sci. 20, 486.

Vissenberg, K., Claeijs, N., Balcerowicz, D., Schoenaers, S., 2020. Hormonal regulation of root hair growth and responses to the environment in Arabidopsis. J. Exp. Bot. 71 (8), 2412–2427.

Kumar, V., Parvatam, G., Ravishankar, GA., 2009. $AgNO_3$ – A potential regulator of ethylene activity and plant growth modulator. Electron. J. Biotechnol. 2, 8-9.

Kundelchuk, OP., Tarasenko, LV., Blume, YB., 2002. Influence of amiprophosmethyl on the root cell structure in the herbicide-sensitive and-resistant lines of *Nicotiana plumbaginifolia*. Russ. J. Plant Physiol. 49 (3), 381-386.

Landi, M., Misra, BB., Muto, A., Bruno, L., Araniti, F., 2020. Phytotoxicity, morphological, and metabolic effects of the sesquiterpenoid nerolidol on *Arabidopsis thaliana* seedling roots. Plants 9, 1347-1366.

Lee, RDW., Cho, HT., 2013. Auxin, the organizer of the hormonal/environmental signals for root hair growth. Front. Plant Sci. 4, 448.

Lei, L., Zhao, Y., Shi, K., Liu, Y., Hu, Y., Shao, H., 2021. Phytotoxic activity of alkaloids in the desert plant *Sophora alopecuroides*. Toxins 13 (10), 706.

Li, X., Mo, X., Shou, H., Wu, P., 2006. Cytokinin-mediated cell cycling arrest of pericycle founder cells in lateral root initiation of Arabidopsis. Plant Cell Physiol. 47, 1112–1123.

Liu, J., Mehdi, S., Topping, J., Friml, J., Lindsey, K., 2013. Interaction of PLS and PIN and hormonal crosstalk in *Arabidopsis* root development. Front. Plant Sci. 4, 75.

Liu, J., Moore, S., Chen, C., Lindsey, K., 2017a. Crosstalk complexities between auxin, cytokinin, and ethylene in *Arabidopsis* root development: from experiments to systems modeling, and back again. Mol. Plant. 10 (12), 1480–1496.

Liu, J., Müller, B., 2017b. Imaging TCSn::GFP, a synthetic cytokinin reporter, in *Arabidopsis thaliana*. Methods Mol. Biol. 1497, 81-90.

López-González, D., Costas-Gil, A., Reigosa, MJ., Araniti, F., Sánchez-Moreiras, AM., 2020. A natural indole alkaloid, norharmane, affects PIN expression patterns and compromises root growth in *Arabidopsis thaliana*. Plant Physiol. Biochem. 151, 378-390.

Lupini, A., Araniti, F., Sunseri, F., Abenavoli, MR., 2014. Coumarin interacts with auxin polar transport to modify root system architecture in *Arabidopsis thaliana*. Plant Growth Reg. 74 (1), 23-31.

Moubayidin, L., Di Mambro, R., Sabatini, S., 2009. Cytokinin-auxin crosstalk. Trends Plant Sci. 14, 557-562.

Na, X., Hu, Y., Yue, K., Lu, H., Jia, P., Wang, H., Wang, X., Bi, Y., 2011. Narciclasine modulates polar auxin transport in Arabidopsis roots. Journal Plant Physiol. 168 (11), 1149-1156.

Negi, S., Ivanchenko, M., Muday, GK., 2008. Ethylene regulates lateral root formation and auxin transport in *Arabidopsis thaliana*. Plant J. 2, 175-187.

Negi, S., Sukumar, P., Liu, X., Cohen, JD., Muday, GK., 2010. Genetic dissection of the role of ethylene in regulating auxin-dependent lateral and adventitious root formation in tomato. Plant J. 61, 3-15.

Oerke, E-C., 2006. Crop losses to pests. J. Agric. Sci. 144 (1), 31-43.

Oono, Y., Ooura, C., Rahman, A., Aspuria, ET., Hayashi, K., Tanaka, A., Uchimiya, H., 2003. p-Chlorophenoxyisobutyric acid impairs auxin response in Arabidopsis root. Plant Physiol. 133, 1135-1147.

Ottenshläger, I., Wolff, P., Wolverton, C., Bhalerao, RP., Sandberg, G., Ishikawa, H., Evans, M., Palme, K., 2003. Gravity-regulated differential auxin transport from columella to lateral root cap cells. Proc. Natl. Acad. Sci. Unit. States Am. 100, 2987-2991.

Qin, H., Huang, R., 2018. Auxin Controlled by Ethylene Steers Root Development. Int. J. Mol. Sci. 19, 3656.

Reed, RC., Brady, SR., Muday, GK. 1998. Inhibition of auxin movement from the shoot into the root inhibits lateral root development in Arabidopsis. Plant Physiol. 118 (4), 1369–1378.

Santos Wagner, AL., Araniti, F., Bruno, L., Ishii-Iwamoto, EL., Abenavoli, MR., 2021. The steroid saponin protodioscin modulates *Arabidopsis thaliana* root morphology altering auxin homeostasis, transport and distribution. Plants 10 (8), 1600.

Schaller, GE., Bishopp, A., Kieber, JJ., 2015. The yin-yang of hormones: cytokinin and auxin interactions in plant development. Plant Cell 1, 44-63.

Shao, H., Huang, X., Zhang, Y., Zhang, C., 2013. Main Alkaloids of *Peganum harmala* L. and their different effects on dicot and monocot crops. Molecules 18, 2623-2634.

Skoog, F., Miller, CO., 1957. Chemical regulation of growth and organ formation in plant tissues cultured *in vitro*. Symp. Soc. Exp. Biol. 11, 118-131.

Su, YH., Liu, YB., Zhang, XS., 2011. Auxin-cytokinin interaction regulates meristem development. Mol. Plant. 4, 616-625.

Tanimoto, M., Roberts, K., Dolan, L, 1995. Ethylene is a positive regulator of root-hair development in *Arabidopsis thaliana*. Plant J. 8, 943-948.

Tranel, PJ., Wright, TR, 2002. Resistance of weeds to ALS-inhibiting herbicides: what have we learned? Weed Sci. 50 (6), 700-712.

Villeneuve, A., Larroudé, S., Humbert JF. 2011. Herbicide contamination of freshwater ecosystems: Impact on microbial communities. In *Pesticides - Formulations, Effects, Fate*, Stoytcheva M (Ed.). InTech Open, 285-312.

Vogel, JP., Schuerman, P., Woeste, K., Brandstatter, I., Kieber, JJ, 1998. Isolation and characterization of *Arabidopsis* mutants defective in the induction of ethylene biosynthesis by cytokinin. Genetics 149, 417–427.

Wightman, F., Schneider, EA., Thimann, KV., 1980. Hormonal factors controlling the initiation and development of lateral roots. II. Effects of exogenous factors on lateral root formation in pea roots. Physiol. Plant. 49, 304–314.

Woeste, K., Vogel, J., Kieber, J, 1999. Factors regulating ethylene biosynthesis in etiolated *Arabidopsis thaliana* seedlings. Physiol. Plant. 105, 478–484.

Zhang, Y., Jiao, Y., Liu, Z., Zhu, YX., 2015. ROW1 maintains quiescent centre identity by confining WOX5 expression to specific cells. Nat. Commun. 6 (1), 1-8.

Figures Captions

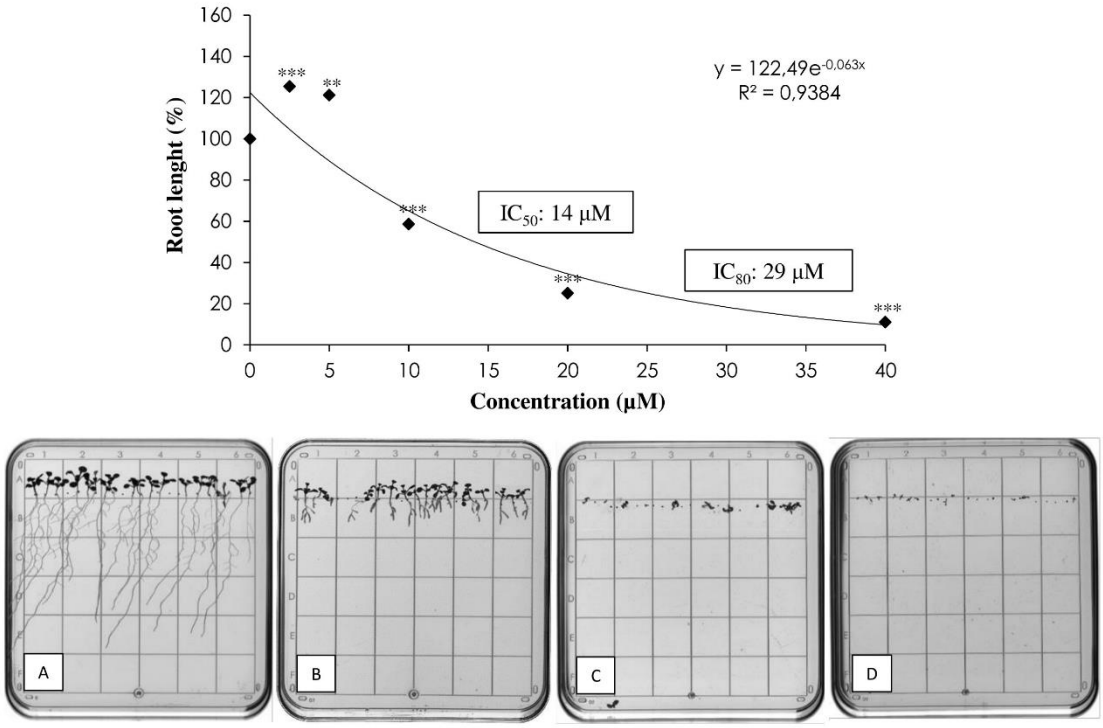

Figure 1. Dose-response curve obtained for radicular length media values of *Arabidopsis thaliana* seedlings treated with different concentrations of harmaline (0, 2.5, 5, 10, 20, 40 and 80 µM). The data are expressed as a percentage of control seedlings growth, in which control growth is represented as 100% (R^2 = 0.9384). Data were analyzed through one way-ANOVA using the Least Significant Differences (LSD, $p \leq 0.05$) test as post-hoc. The asterisks indicate significant differences compared to control: (* $p \leq 0.05$; ** $p \leq 0.01$; *** $p \leq 0.001$). The images show *Arabidopsis thaliana* seedlings

growing in contact with 0 **(A)**, 20 **(B)**, 50 **(C)** and 400 **(D)** µM harmaline. N=5 (each replicate is a bulk of 24 plants).

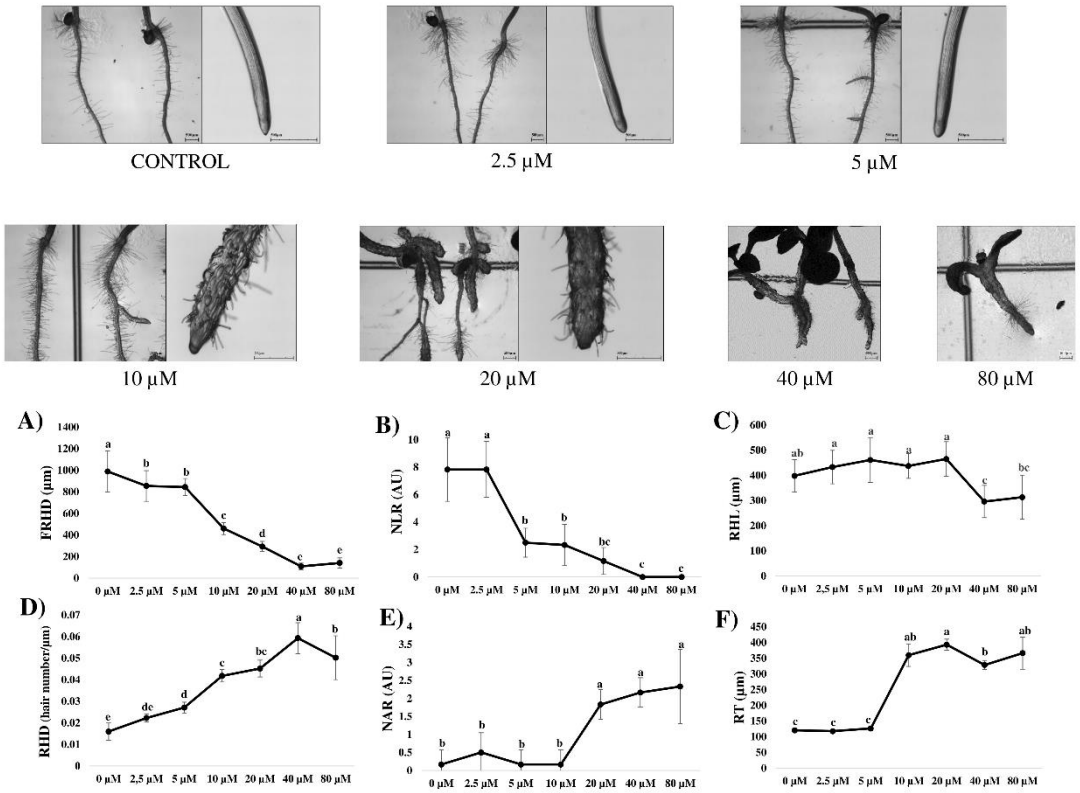

Figure 2. Effects of harmaline on root morphology of *Arabidopsis thaliana*.**(A)** First root hair distance (FRHD), **(B)** Number of lateral roots (NLR), **(C)** Root hairs length (RHL), **(D)** Root hairs density (RHD), **(E)** Number of adventitious roots (NAR), **(F)** Root thickness (RT) of *A. thaliana* seedlings treated with 0, 2.5, 5, 10, 20, 40 and 80 µM after 14 days of growth. Data were statistically analyzed through t-test with $P \leq 0.05$. Different letters indicate significant differences between treatments. N=5.

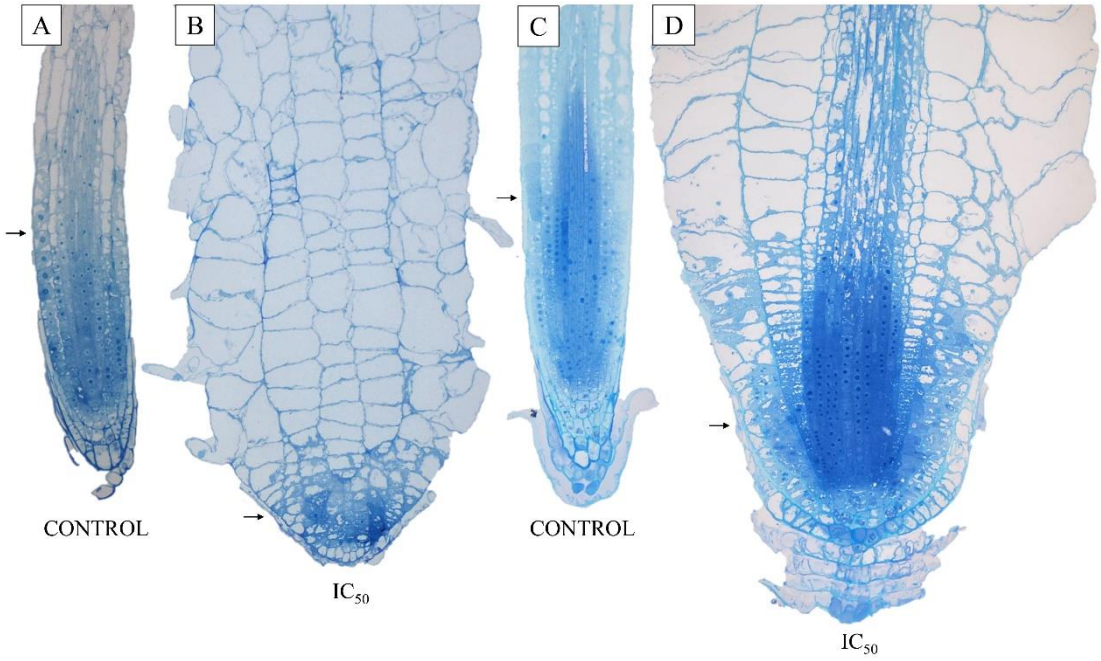

Figure 3. Longitudinal sections of the apical region of *Arabidopsis thaliana* roots treated with harmaline and visualized under light microscopy. **(A)** Control root after 7 days of growth. **(B)** IC_{50} harmaline-treated root after 7 days of growth. **(C)** Control root after 14 days of growth. **(D)** IC_{50} harmaline-treated root after 14 days of growth. All the images were taken under 20X magnification. Black arrows indicate the final of the apical meristem (transition zone).

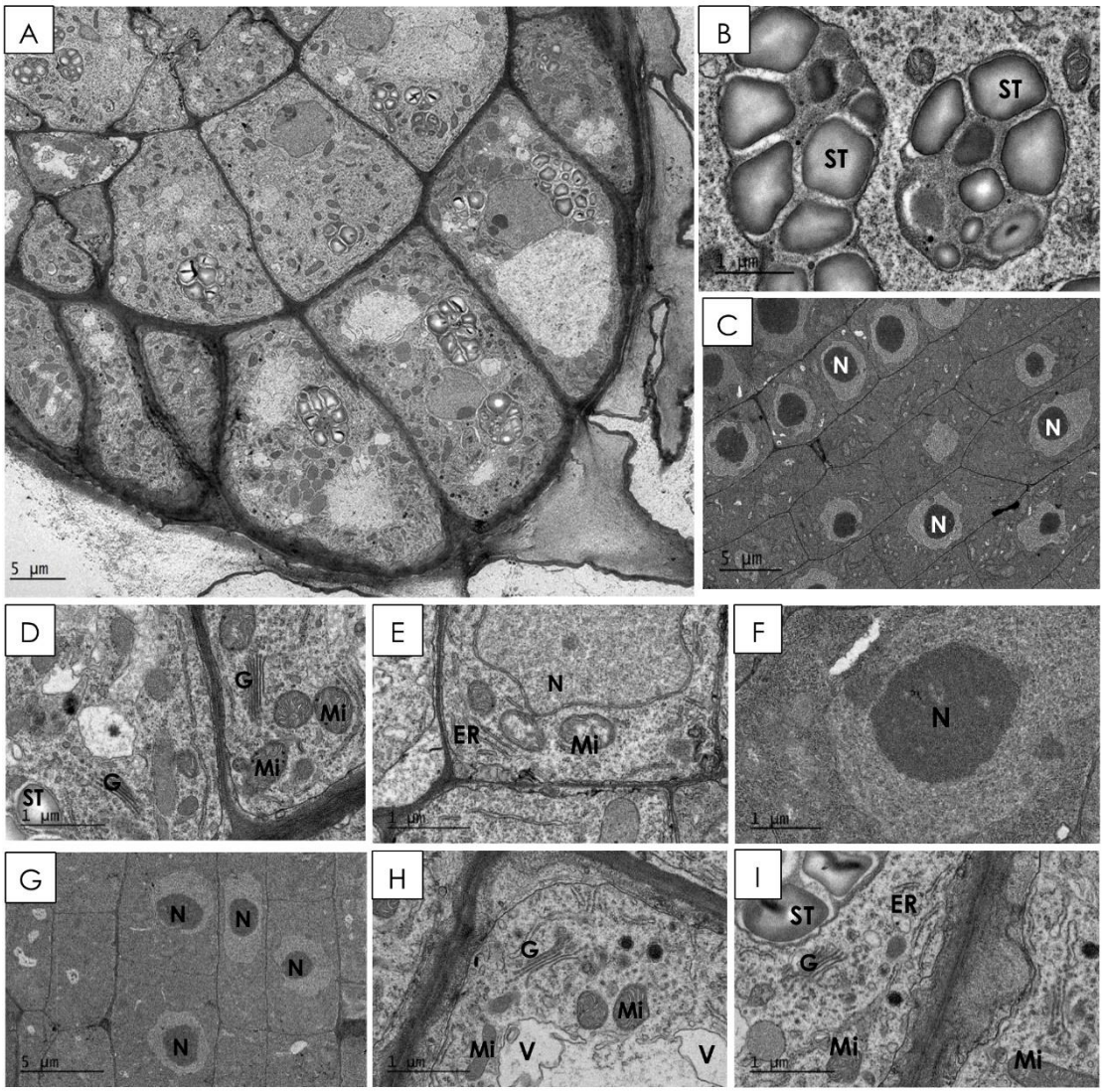

Figure 4. Images of transmission electron microscopy (TEM) of control *Arabidopsis thaliana* roots after 7 (A-E) and 14 (F-I) days of growth. **(A)** Columella of control seedling. **(B)** Well defined statoliths. **(C, G)** Dividing cells with spheric and regular nuclei. **(D, E, H, I)** Different organelles in a control cell (N: nuclei, V: vacuole, ER: endoplasmic reticulum, MI: mitochondrion, ST: statoliths, G: Golgi). **(F)** Nuclei. Scale bars: figures A, C and G, 5 µm; figures B, C, D, E, H and I, 1 µm. N=3.

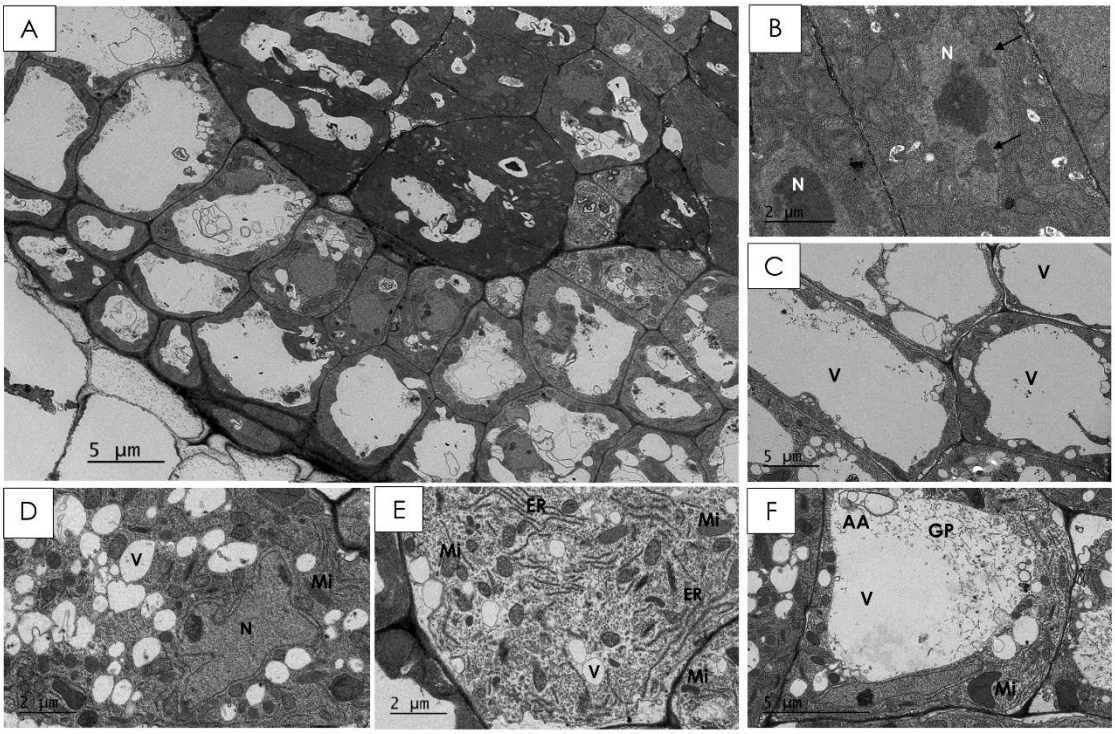

Figure 5. Images of transmission electron microscopy (TEM) *Arabidopsis thaliana* roots treated with IC_{50} harmaline for 7 days. **(A)** Columella of treated seedling. **(B)** Nuclei with fragmented chromatin. **(C)** Massive vacuolization in meristematic zone. **(D, E, F)** Different organelles in treated cell (N: nuclei, V: vacuole, ER: endoplasmic reticulum, MI: mitochondrion, GP: vacuole granular precipitate). Scale bars: figures A, C and F, 5 µm; figures B, D, E, 2 µm. Black arrows indicate fragmented chromatin. N=3.

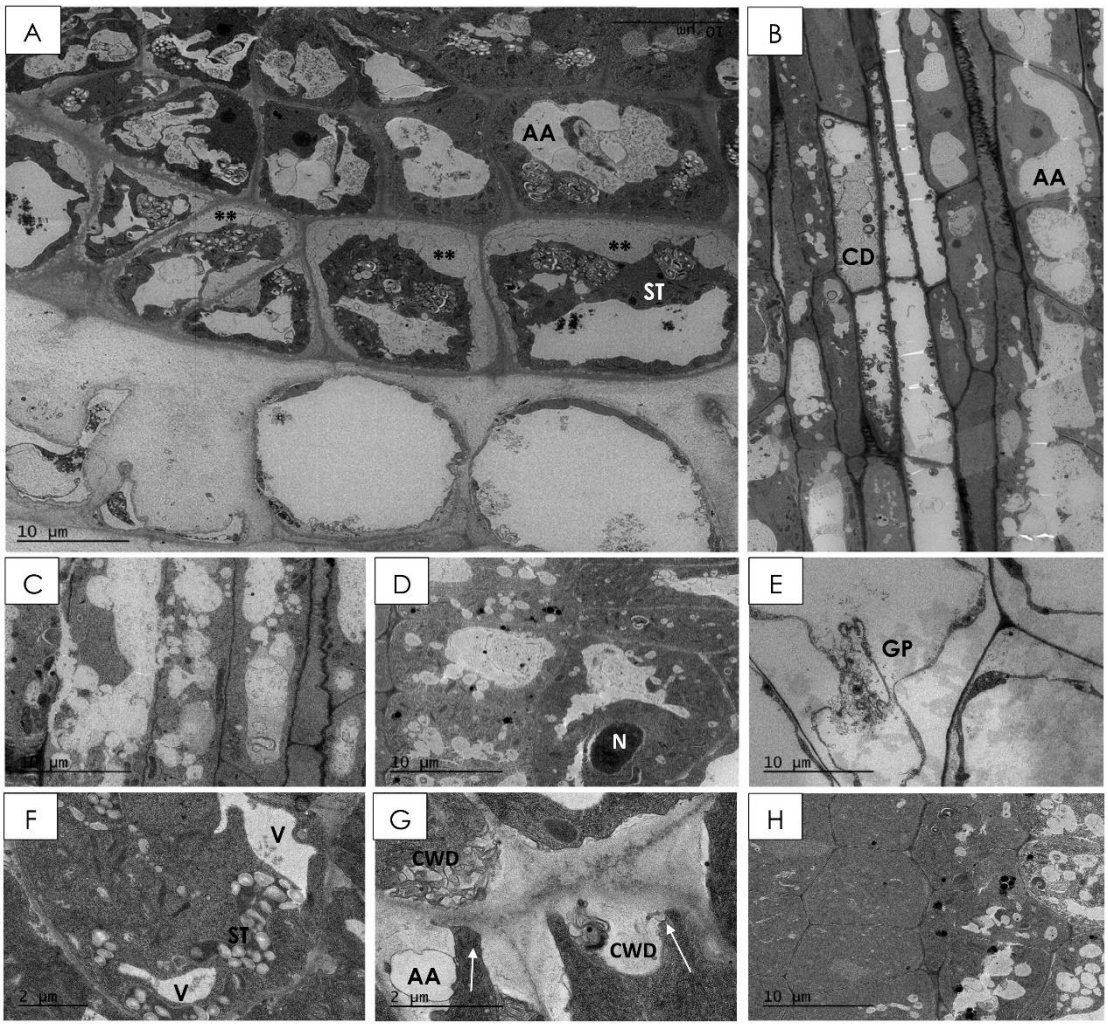

Figure 6. Images of transmission electron microscopy (TEM) *Arabidopsis thaliana* roots treated with IC_{50} harmaline for 14 days. **(A)** Columella of treated seedling. **(B)** Vascular tissue in stele. **(C, D, H)** Dividing cells with vacuoles and irregular nuclei. **(E)** Vacuolization of meristematic zone **(F)** Disorganized statoliths **(G)** Deformed cell wall with deposits. **: detached cytoplasm; CD: cytoplasm degradation; AA: autolytic activity; GP: vacuole granular precipitate; CWD: cell wall deposit. White arrows indicate deformed cell wall. Scale bars: figures A, B, C, D, E, H 10 µm; figures F and G 2 µm. N=3.

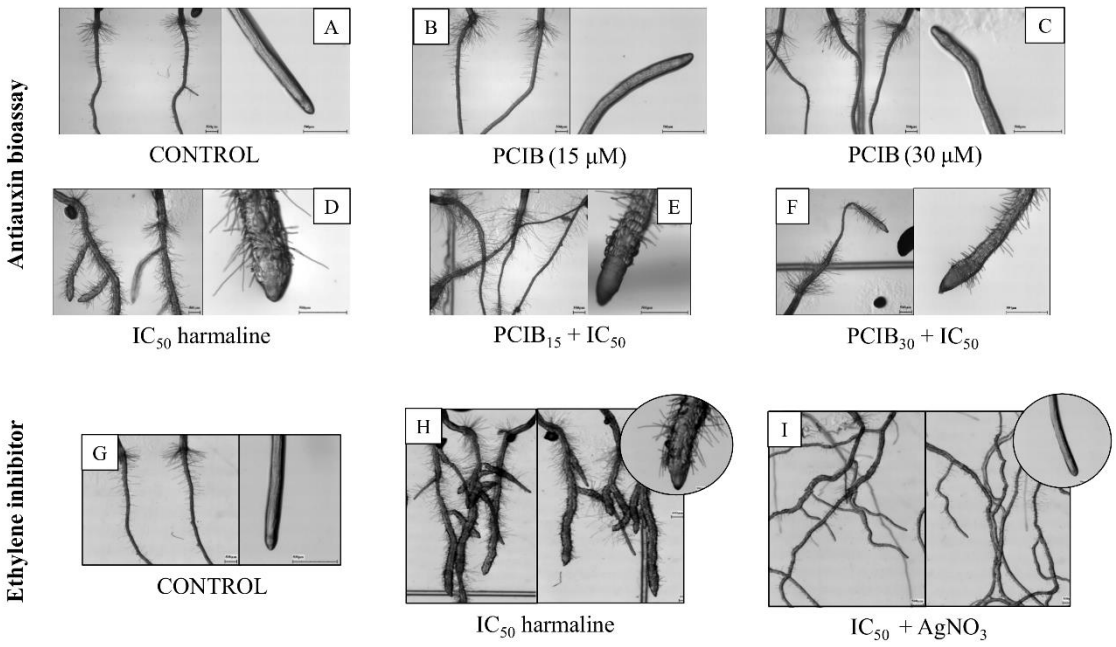

Figure 7. *Arabidopsis thaliana* seedling roots treated with IC_0 (0 µM) harmaline **(A, G)**; IC_{50} harmaline (14 µM) **(D, H)**; PCIB (15 µM) **(B)**; PCIB (30 µM) **(C)**; $PCIB_{15}$ + IC_{50} harmaline **(E)**; $PCIB_{30}$ + IC_{50} harmaline **(F)** and IC_{50} harmaline + $AgNO_3$ **(I)** visualized under stereo-microscopy after 14 days of growth. N=5.

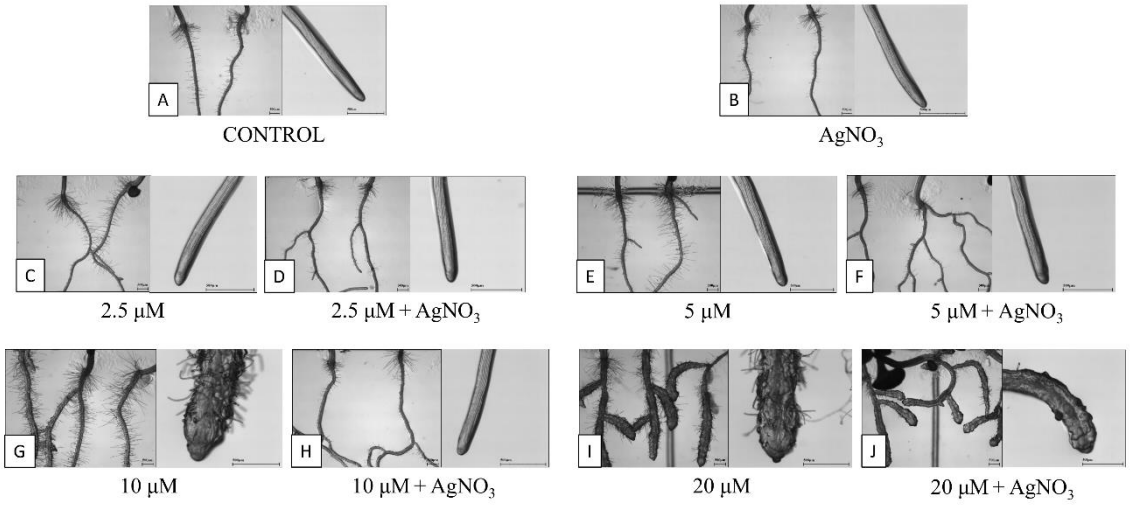

Figure 8. *Arabidopsis thaliana* seedling roots treated with 0 µM harmaline **(A)**; $AgNO_3$ (10 µM) **(B)**; 2.5 µM harmaline **(C)**; 2.5 µM + $AgNO_3$ **(D)**; 5 µM harmaline **(E)**; 5 µM + $AgNO_3$ **(F)**; 10 µM harmaline **(G)**; 10 µM + $AgNO_3$ **(H)**; 20 µM harmaline **(I)** and 20 µM + $AgNO_3$ **(J)** visualized under stereo-microscopy after 14 days of growth. N=5.

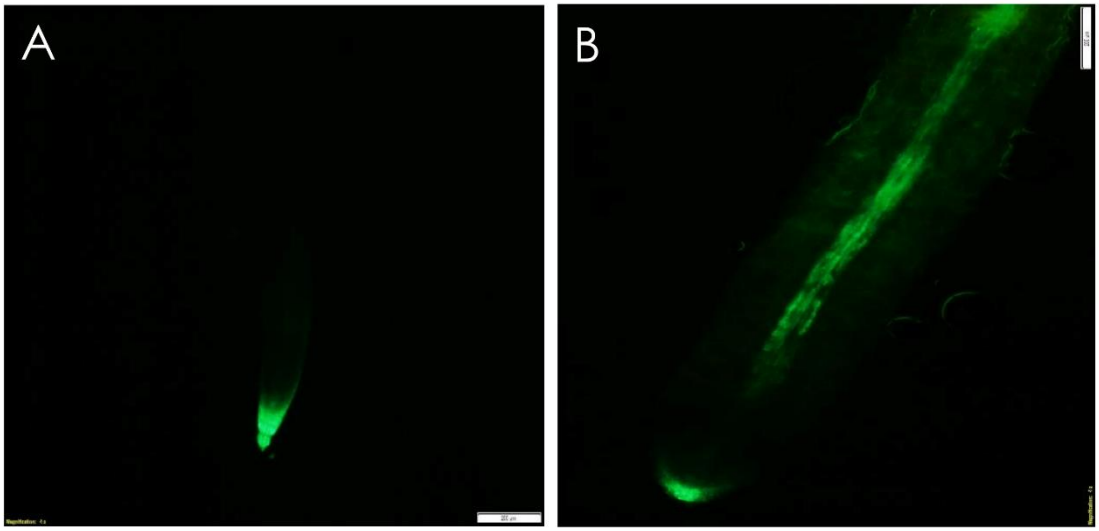

Figure 9. *Arabidopsis thaliana* root of *pTCSn::GFP* seedlings treated with IC_0 (0 μM) **(A)** and IC_{50} harmaline (14 μM) **(B)**, and both visualized (20X magnification) under confocal microscopy (Leica TCS SP5) after 14 days of growth. N=5.

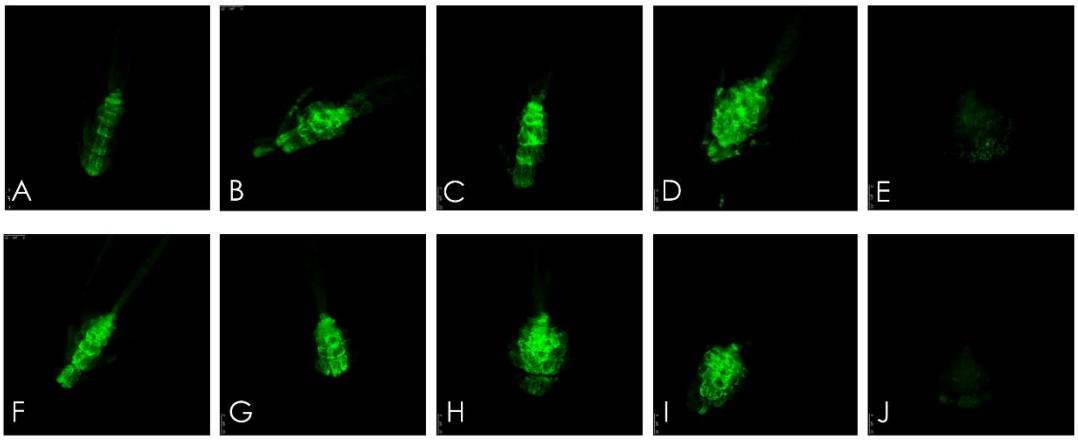

Figure 10. *Arabidopsis thaliana* root of *pDR5::GFP* seedlings treated with 0, 2.5, 5, 10 and 20 μM harmaline (**A-E**, respectively) and 0, 10, 13, 16 and 19 μM harmaline (**F-J**, respectively) visualized (63X magnification) under confocal microscopy (Leica TCS SP5) after 14 days of growth. N=5.

Table 1. Quantification of changes detected in the cell structure and the organelles of untreated (0 µM) and harmaline-treated (14 µM) *Arabidopsis* roots after 7 and 14 days of growth.

Observations	7 days of growth		14 days of growth	
	Control	**IC_{50} (14 µM)**	**Control**	**IC_{50} (14 µM)**
Cell wall thickness	0.117 ± 0.024	0.278 ± 0.08***	0.152 ± 0.034	0.916 ± 0.539***
Golgi apparatus secretory activity	1.6 ± 1.57	2.6 ± 1.51	0.9 ± 1.1	11.8 ± 3.79***
Percentage of aberrant nuclei	21.89 ± 2.71	56.62 ± 5.95***	25.64 ± 5.12	59.97 ± 5.42***
Density of mitochondria	15.2 ± 4.61	21 ± 5.59*	12.5 ± 3.31	17.6 ± 2.95**
Density of altered mitochondria	0.6 ± 0.69	2.6 ± 0.69***	0.3 ± 0.48	2 ± 0.86***
Density of vacuoles	0.9 ± 1.1	12.7 ± 5.54***	0.9 ± 0.73	13.2 ± 3.01***
Percentage of cell with wall deposits	17.48 ± 2.92	56.39 ± 6.85***	15.31 ± 3.72	56.11 ± 5.35***

Ultrastructure measurements were expressed as: cell wall thickness (µm); Golgi apparatus secretory activity (nº of vesicles / Golgi); percentage of aberrant nuclei (nº aberrant nuclei / 10 cell x 100); density of mitochondria (nº of mitochondria / cell); density of altered mitochondria (nº altered mitochondria / cell); density of vacuoles (nº vacuoles / cell); percentage of cell with wall deposits (nº of cell with wall deposits / 10 cell x 100). Data were expressed as means ± SD. Differences between treatments were statistically analysed through t-test with $P \leq 0.05$. N=10. Asterisks indicate significant differences compared to the control: * = ($P \leq 0.05$); ** = ($P \leq 0.01$); *** = ($P \leq 0.001$).